Chapter 2

Magneto-Plasmonics and Optical Activity in Graphene-Based Nanowires

Dmitry A. Kuzmin, Igor V. Bychkov,
Vladimir G. Shavrov and Vasily V. Temnov

Additional information is available at the end of the chapter

http://dx.doi.org/10.5772/67417

Abstract

Nowadays, graphene plasmonics shows a great number of features unusual for traditional (metal-based) plasmonics from high localization and large propagation distance of surface plasmon-polaritons (SPPs) through the existence of both TE- and TM-polarized SPPs to the possibility of controlled SPPs by graphene chemical potential (or, equivalently, by gate voltage or chemical doping). Cylindrical graphene-based plasmonic structures have some advantages in contrast to planar geometry: absence of edge losses, existence of high-order azimuthal modes, etc. In this work, we discuss some ways to obtain an optical activity in cylindrical graphene-based plasmonic structures and its possible applications to SPPs manipulation.

Keywords: surface plasmon-polaritons, graphene, optical activity, magneto-plasmonics, metasurface

1. Introduction

Nowadays, it is evident that graphene is a very promising material for many optics, photonics and plasmonics applications [1–3]. Graphene layers (single layer as well as two- and multi-layer waveguides) may support highly localized electromagnetic waves, i.e. surface plasmon-polaritons (SPPs), both TE and TM polarized [4–9]. Tight confinement and large propagation length of plasmons make it possible to observe strong light-matter interactions in graphene-based structures [10]. Practically, only graphene ribbons of finite weight may be used. Unfortunately, the edges of such ribbons lead to undesirable increase in losses [11]. The possible way to solve this problem is the use of cylindrical 2D surfaces [12]. Graphene-based cylindrical waveguides may operate in single- and multi-mode regimes in the frequency range from THz to mid-IR [13–15]. They may support TE-polarized plasmons [16], similar to the single graphene layer [4].

For realizing any plasmonic devices, one should have the instrument for manipulating by plasmon-polaritons. This goal may be achieved, for example, by the combination of plasmonic and optically active materials [17–22]. Among other optically active materials, the use of magnetic ones leads to cross-coupling between magnetic properties of materials and optical fields: different mechanisms may lead to optically induced magnetic fields [23–26] and excitation of localized plasmons may lead to a major increase in magneto-optical effects [27–31].

It is well known that magnetic field (or magnetization) in cylindrical optical fibres may lead to the rotation of the energy distribution (i.e. speckle-pattern) into cross-section of the fibre [32–35]. The nature of this effect is magnetic field-induced breaking of degeneracy of the modes with opposite signs of azimuthal mode index (i.e. rotating in opposite azimuthal directions). Recently, we have shown that in graphene-coated optical fibre one may control such rotation by both magnetic field and chemical potential of the graphene [36], but for observable rotation it is necessary that the fibre length should be of a few centimetres. Recently, we have shown that in case of magneto-active nanowire covered by graphene layer one may achieve the rotation of some plasmonic modes by up to ~100° on the scale of about 500 nm at mid-infrared frequencies [37]. Tuning carrier concentration in graphene by chemical doping or gate voltage allows controlling of SPP properties and notably the rotation angle of high-order azimuthal modes.

In this chapter, we summarize our previous results and discuss some magnetic-free ways to obtain similar effects. Our results may open the door for the application of straintronic control in plasmonics and the design of one-way propagation plasmonic devices.

The chapter consists of introduction, three sections and conclusions. In Section 2, we review basic properties of SPPs propagating in cylindrical graphene-based plasmonic waveguides. We discuss conditions of propagation of both TM and TE fundamental modes and TM-like high-order SPPs. This section also covers some features of effective magnetic field induced via inverse Faraday effect. In Section 3, we show the possibility of rotation of SPPs, which are supported by graphene-coated gyrotropic nanowire. Section 4 discusses the similar effects of the spiral graphene-based plasmonic waveguide.

2. Surface plasmon-polaritons in graphene-covered nanowires

Cylindrical graphene-based plasmonic waveguides of different configurations have been well investigated in the literature [13–16]. It has been shown that such a waveguide may support high-order azimuthal plasmonic modes and may work in the single-mode regime.

Let us consider a nanowire with the dielectric permittivity $\varepsilon_{\text{wire}}$ covered by a graphene layer. This structure is embedded in the medium with permittivity ε_{out}. The radius of nanowire is R. We will use cylindrical coordinates (r, ϕ, z). The nanowire axis is supposed to be the z-axis. We describe graphene by a 2D conductivity σ_g [38], which depends on the temperature T, the angular frequency ω, the scattering rate Γ and the chemical potential (or the Fermi energy) $\mu_{\text{ch}} \approx \hbar v_F(\pi n)^{1/2}$, where $v_F \approx 10^6$ m/s is the Fermi velocity. For example, $n \approx 8 \times 10^{13}$ cm^{-2} corresponds $\mu_{\text{ch}} \approx 1$ eV. We use a standard model of graphene surface conductivity calculated within the local random phase approximation with the dominant Drude term at SPP energies below the Fermi level [39, 40].

We will consider monochromatic plasmons propagating along the nanowire axis (*z*-axis) by putting electric and magnetic fields $\mathbf{E}, \mathbf{H} \propto \exp[i(\beta z - \omega t)]$ into Maxwell's equations ($\beta = \beta' + i\beta''$ is a complex propagation constant, ω is a circular frequency). Components of electric and magnetic fields in the cylindrical coordinates (r, ϕ, z) inside the nanowire (i.e. at $0 < r < R$) are the following:

$$\begin{aligned}
E^{\text{in}}_{r,m} &= -ig^{-2}\{\beta g A_m I'_m(gr) + i\omega m\mu_0 r^{-1} B_m I_m(gr)\},\\
E^{\text{in}}_{\phi,m} &= -ig^{-2}\{i\beta m r^{-1} A_m I_m(gr) - \omega\mu_0 g B_m I'_m(gr)\},\\
E^{\text{in}}_{z,m} &= A_m I_m(gr),\\
H^{\text{in}}_{r,m} &= -ig^{-2}\{\beta g B_m I'_m(gr) - i\omega m\varepsilon_{in} r^{-1} A_m I_m(gr)\},\\
H^{\text{in}}_{\phi,m} &= -ig^{-2}\{i\beta m r^{-1} B_m I_m(gr) - \omega\varepsilon_{in} g A_m I'_m(gr)\},\\
H^{\text{in}}_{z,m} &= B_m I_m(gr).
\end{aligned} \tag{1}$$

In Eq. (1), a multiplier $\exp[i(m\phi + \beta z - \omega t)]$ has been omitted. Equations describing fields outside the nanowire (at $r > R$) $\mathbf{E}^{\mathbf{out}}$, $\mathbf{H}^{\mathbf{out}}$ may be derived from Eq. (1) by substitutions:

$$g \to p, I_m(gr) \to K_m(pr), A_m \to C_m, B_m \to D_m,\ \varepsilon_{\text{in}} \to\ \varepsilon_{\text{out}}. \tag{2}$$

In all formulae, $I_m(x)$ and $K_m(x)$ are modified Bessel's functions of the first and second types, respectively; operation ′means differentiation with respect to the argument; $g^2 = \beta^2 - \omega^2\varepsilon_{\text{in}}\mu_0$, $p^2 = \beta^2 - \omega^2\varepsilon_{\text{out}}\mu_0$, where μ_0 is the magnetic constant. Parameters p and g are related to the field confinement of mode. Constants A_m, B_m, C_m and D_m are determined by boundary conditions and mode normalization procedure. The boundary conditions at $r = R$ are the following: $E^{\text{in}}_{z,m} = E^{\text{out}}_{z,m}$, $E^{\text{in}}_{\varphi,m} = E^{\text{out}}_{\varphi,m}$, $H^{\text{out}}_{z,m} - H^{\text{in}}_{z,m} = -\sigma_g E^{\text{in}}_{\varphi,m}$ and $H^{\text{out}}_{\varphi,m} - H^{\text{in}}_{\varphi,m} = \sigma_g E^{\text{in}}_{z,m}$.

The characteristic (or dispersion) equation for the mth plasmonic mode may be obtained from boundary conditions with fields expressions (1) and (2).

For $m = 0$, electromagnetic waves may be classified into TE and TM modes. High-order modes have all non-zero components of electric and magnetic fields.

Dispersion relation for TE-polarized fundamental mode ($m = 0$) reads [16]

$$i\omega\mu_0\sigma_g = \frac{gI_0(gR)}{I_1(gR)} + \frac{pK_0(pR)}{K_1(pR)}. \tag{3}$$

Both terms on the right-hand side are positive; so, we may conclude that condition $\text{Im}[\sigma_g] < 0$ is necessary. But this condition is not sufficient. Let us suppose that $|\text{Re}[\sigma_g]| << |\text{Im}[\sigma_g]|$. This condition is satisfied near the inter-band transition (i.e. when $1.667 < \hbar\omega/\mu_{\text{ch}} < 2$). Cut-off limit (i.e. $p \to 0$) leads to critical coupling among the core radius, frequency and dielectric permittivity. The limit $g_{cr}R << 1$, which corresponds to small core radius, small difference of permittivities of the inner and the outer mediums, or low frequency, leads to the condition of $\omega\mu_0|\text{Im}[\sigma_g]|R = 2$. Estimations of critical radius for the frequency range 100–600 THz (near-infrared to visible light) give $R \sim 1$ μm.

High-order TE-like SPPs modes may propagate in the structures with much larger radius, and, thus, are of interest for practical plasmonic applications.

TM-SPPs have been investigated in details in [13, 14]. Dispersion relation of TM fundamental plasmonic modes is

$$\frac{\varepsilon_{\text{out}} K_0(pR)}{pK_1(pR)} + \frac{\varepsilon_{in} I_0(gR)}{gI_1(gR)} + i\frac{\sigma_g}{\omega} = 0. \tag{4}$$

This mode exists for any radius values and frequencies of electromagnetic wave, when $\text{Im}[\sigma_g] > 0$.

The modes with index $|m| > 0$ exist above the cut-off frequency. The number of supported modes at the fixed vacuum wavelength λ_0 may be estimated as $\text{Re}[i2\pi R(\varepsilon_{\text{wire}}+\varepsilon_{\text{out}})c/(\sigma_g\lambda_0)]$. An increase of the core permittivity leads to an increase in the number of supported modes.

Comparison of the SPPs characteristics of graphene-covered nanowire and gold-coated nanowire in the frequency range of 30–50 THz shows [13] that the effective mode index of SPPs mode in graphene-covered nanowire is much larger than that of gold-coated nanowire, indicating that plasmon mode in graphene-covered nanowire has a much shorter SPP wavelength and better mode confinement. SPPs mode in graphene-covered nanowire has a much smaller mode area: the mode energy of graphene-covered nanowire is mainly localized inside the nanowire, while the mode energy of gold-coated nanowire resides outside the Au coating.

Field expressions (1) with (2) allow one to calculate the inverse magneto-plasmonic effect [41]: i.e. the effective magnetic field induced by propagating SPPs due to the inverse Faraday effect $\mathbf{H}_{\text{eff}} = \alpha\text{Im}[\mathbf{E}\times\mathbf{E}^*]$. For mode with $m = 0$ SPPs may be classified into TE and TM modes. It is easy to show that TE mode cannot produce any magnetic field, while TM mode can induce azimuthal magnetic field. Magnetic field components induced by any single mode do not depend on the azimuthal angle ϕ. For modes with $m \neq 0$, all components of magnetic field are non-zero. Change in the propagation direction leads to a change in the $\mathbf{H}_{\text{eff}}$ rotation direction. Modes with greater $|m|$ induces longitudinal component of magnetic field as well. The value of this component increases with an increase in mode number. We have found also that in two-mode regime it is possible to induce azimuthally periodic magnetic field distribution. This distribution may be rotated by these two mode phase shift controls.

3. Gyrotropic graphene-coated nanowires

Let us consider a gyrotropic nanowire covered by a graphene layer (see **Figure 1**). We will use cylindrical coordinates (r, ϕ, z). The nanowire axis is supposed to be the z-axis, which coincides with the gyration axis. Such situation may be realized, for example, in magnetic nanowires magnetized along the wire axis. The electrodynamic properties of the nanowire may be described by the following dielectric permittivity tensor:

$$\hat{\varepsilon}_{\text{wire}} = \varepsilon_0 \begin{pmatrix} \varepsilon_\perp & -i\varepsilon_a & 0 \\ i\varepsilon_a & \varepsilon_\perp & 0 \\ 0 & 0 & \varepsilon_\parallel \end{pmatrix} \tag{5}$$

http://dx.doi.org/10.5772/67417

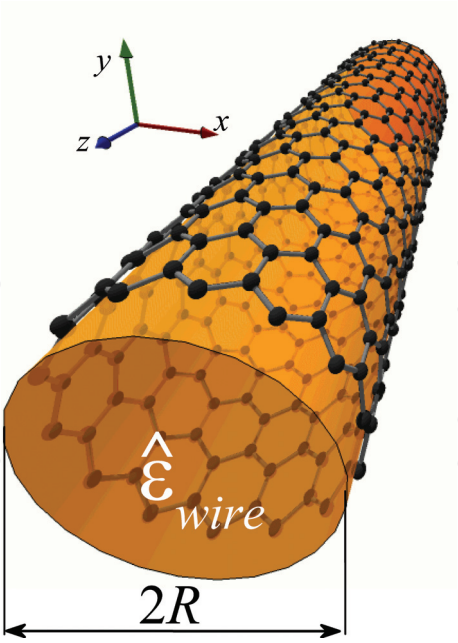

Figure 1. Geometry of the problem.

Here, ε_0 is the electric constant (we will use SI units throughout the chapter). Graphene layer may be described by 2D conductivity σ_g, which depends on the temperature T, the angular frequency ω, the scattering rate Γ and the chemical potential μ_{ch}. It may be calculated in local random phase approximation [39, 40], for example. We will take into account the presence of graphene only as a specific boundary condition [38]. We will suppose that the outer medium is the air, i.e. it has dielectric permittivity $\varepsilon_{out} = \varepsilon_0$.

Characteristics of SPP modes propagating in graphene-covered non-gyrotropic nanowire have been investigated in details [13–16]. In Section 2, it has been discussed that plasmonic modes in such structure may induce a complex distribution of magnetic field via inverse Faraday effect. Here, we suppose that intensity of plasmonic modes under consideration is small enough, and one may neglect the inverse Faraday effect inside magnetic nanowire.

Now, one has to solve Maxwell's equations inside each medium. We suppose that electromagnetic wave has harmonical time dependence and propagates along the z-axis, i.e. $\mathbf{E}, \mathbf{H} \sim \exp[-i\omega t + i\beta z]$, where $\beta = \beta' + i\beta''$ is a complex propagation constant. Electromagnetic field distribution inside magnetic nanowire with permittivity tensor (Eq. (5)) may be expressed similarly to that of circular microwave waveguides and optical fibres filled by gyrotropic medium [42–44]. Field outside the nanowire has a usual form (see Eqs. (1) and (2)). These fields should satisfy the boundary conditions at $r = R$: $E^{in}_{z,m} = E^{out}_{z,m}$, $E^{in}_{\varphi,m} = E^{out}_{\varphi,m}$, $H^{out}_{z,m} - H^{in}_{z,m}$

$= -\sigma_g E^{in}_{\varphi,m}$ and $H^{out}_{\varphi,m} - H^{in}_{\varphi,m} = \sigma_g E^{in}_{z,m}$. So, we will have the dispersion equation. Solving this equation, one will obtain β for each azimuthal mode index m.

Standard characteristics of SPP are the SPP wavelength $\lambda_{SPP} = 2\pi/\beta'$, and propagation length $L_{SPP} = (\beta'')^{-1}$. When L_{SPP} becomes less than λ_{SPP} for chosen m, the corresponding SPP mode becomes overdamped and cannot propagate in the structure.

Analytical analysis shows that dispersion equation has terms with the first and third powers of the mode index m. This leads to non-reciprocity for modes with the opposite azimuthal propagation direction, i.e. modes with different signs of m will propagate with slightly different velocities.

Let us suppose that at $z = 0$ one has a field distribution with azimuthal dependence $\sim\cos(m\phi)$. Such distribution may be described by superposition of two modes with $m = \pm|m|$, which are excited without phase shift:

$$E_i = \tilde{E}_{i,+m}(r)\exp[im\phi]exp[i\beta_{+m}z] + \tilde{E}_{i,-m}(r)\exp[-im\phi]exp[i\beta_{-m}z] \quad (6)$$

where $\tilde{E}_{i,\pm m}(r)$ are the radial distributions of the field, $i = r, \varphi, z$. Indeed, due to the difference between propagation constants $\beta_{\pm m}$, this distribution will differ for opposite signs of m, but in the first approach we will suppose that $\tilde{E}_{i,+m}(r) \approx \tilde{E}_{i,-m}(r)$. Correctness of such assumption will further be approved by numerical calculations of field distributions. Different values of propagation speed will lead to phase shift at chosen $z = z_0$ and, thus, to the rotation of field distribution on the angle $(\beta'_{-m} - \beta'_{+m})z_0/2m$. This formula is similar to the one for microwave waveguide filled by gyrotropic medium [43]. For the characterization of rotation angle, we will use the specific rotation angle for each mode defined as following:

$$\theta = \frac{\beta'_{-m} - \beta'_{+m}}{2m}. \quad (7)$$

Propagation length will also differ for modes with opposite signs of m. This may lead to the fact that at certain value of z, one of the modes becomes negligibly small. At such length, defined by the condition

$$|\beta''_{-m} - \beta''_{+m}|z_0 >> 1, \quad (8)$$

the initial azimuthal intensity distribution becomes spatially homogeneous.

For numerical solution of dispersion equation and investigation of field distributions, we will use the following parameters: linear frequency of electromagnetic wave $f = \omega/2\pi = 100$ THz (wavelength in vacuum $\lambda_0 = 3$ μm), nanowire radius $R = 50$ nm (quantum effects in graphene structures should be taken into account at the size of the structure less than ≈20 nm [45]). For simplicity, we will assume that $\varepsilon_\perp = \varepsilon_{||} = \varepsilon$. The value of ε will be set at 2. We will consider the room temperatures ($T = 300$ K) and graphene scattering rate $\Gamma = 0.1$ meV. Due to the fact that rotation may be observed only for modes that depend on azimuthal angle, we will consider the modes with $|m| \neq 0$.

Figure 2 shows the electric field distribution of some high-order modes at z = 100 nm for different values of ε_a. Graphene chemical potential is μ_{ch} = 1 eV. Dash-dot lines show the calculated position of maximum. One can see that the calculated rotation angles are in good agreement with numerical modelling. Change in the sign of gyrotropy ε_a (i.e. change in magnetization or magnetic field direction) leads to opposite rotation of field distribution. The difference between radial distributions of the fields with opposite signs of m has no evident effect. For high-index modes in giant gyrotropy case, condition (8) is not satisfied, and one can see the blurring of distribution we have mentioned above.

A change in graphene conductivity (or its chemical potential) may lead to greater difference in propagation constants of the modes with opposite signs of m. This may be used for adjusting the rotation angle, similarly to graphene-covered optical fibre [36]. Dependences of the specific rotation angle, calculated by Eq. (7) for some lower modes, are shown in **Figure 3**. This figure also contains SPP wavelength and propagation length. One can see that specific rotation angle reaches a maximum at certain chemical potential, for which values are different for each mode. For lower modes, the maximum corresponds to higher chemical potential values. These maximal values are indicated by dashed lines. Maximal rotation angle decreases when mode number increases. An increase in gyrotropy $|\varepsilon_a|$ leads to some shift of the maximum to lower chemical potentials. For positive values of gyrotropy, the specific rotation angles are negative but equal to the absolute value in the case of negative gyrotropy. For the graphs of SPP

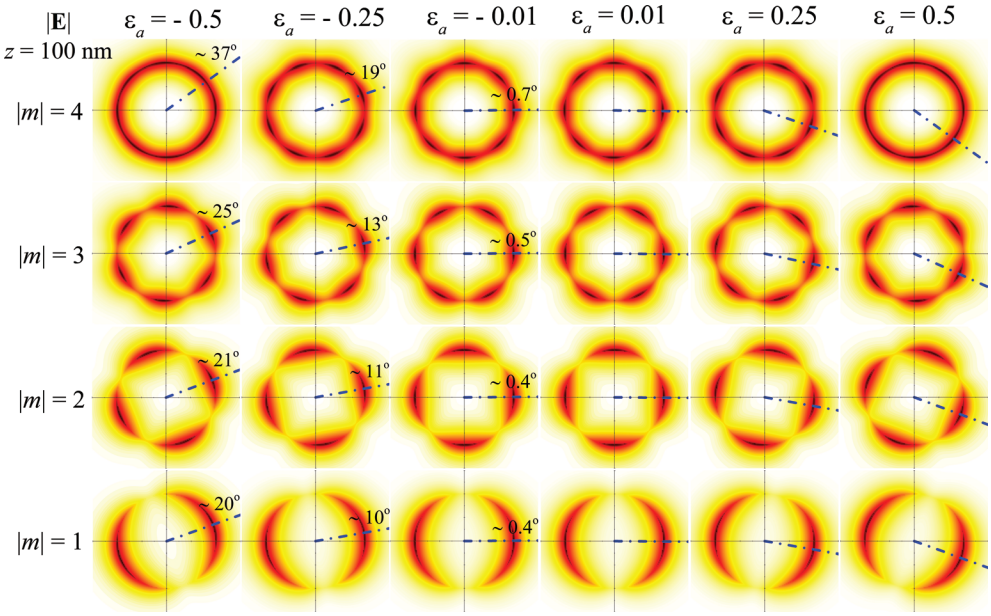

Figure 2. Electric field distribution of some lower modes at z = 100 nm for different values of ε_a. Dash-dot lines show the calculated position of the first maximum. Calculated rotation angles are shown as well. For $\varepsilon_a > 0$ rotation angles are the same as for corresponding case of $\varepsilon_a < 0$, but distribution rotates in opposite direction. Graphene chemical potential is μ_{ch} = 1 eV.

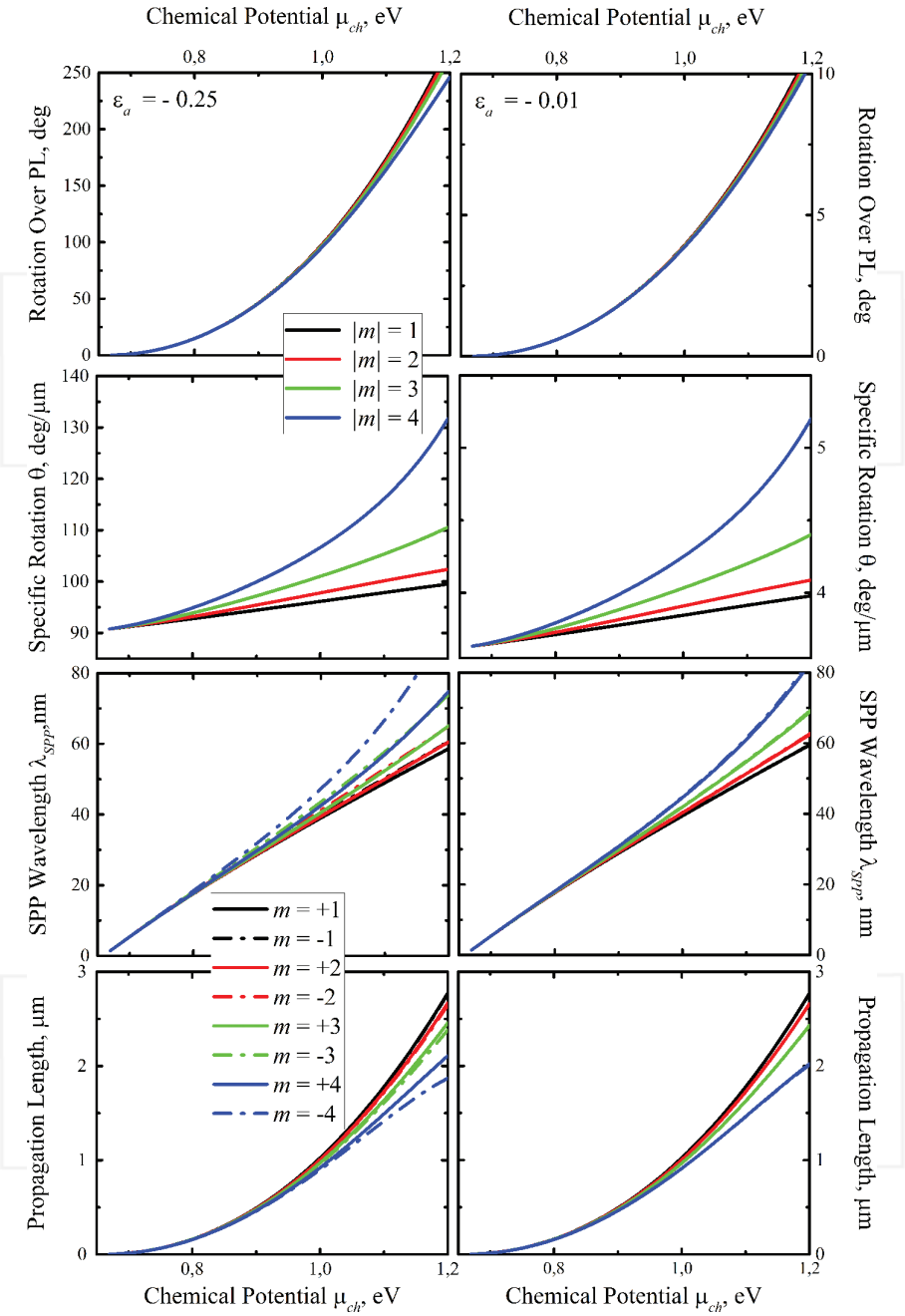

Figure 3. Dependences of the specific rotation angle, SPP wavelength and propagation length versus chemical potential of graphene. The vertical dashed lines show the position of maximum of specific rotation angle for corresponding mode.

wavelength and propagation length change, the sign of ε_a leads to the exchange of the lines for $m > 0$ and $m < 0$.

In general, the specific rotation angle may be adjusted approximately twice by changing the chemical potential of graphene.

It should be noted that the maximal specific rotation is observed near the inflection point of dependence of SPP wavelength versus chemical potential for the mode with higher wavelength. At such chemical potential values, corresponding modes have propagation length less than SPP wavelength, i.e. when the modes become evanescent. One can also see that for maximal rotation angles propagation lengths of the modes with opposite sign of m differ significantly. Thus, condition (8) plays a crucial role.

Propagation characteristics of the modes depend on the permittivity of nanowire, its radius and frequency of electromagnetic wave. All these values may be used for achieving the maximal rotation of desirable mode, but this question needs to be investigated separately.

Rotation angle linearly depends on the length of nanowire. So, the maximal rotation may be reached at the propagation length of SPPs. But one has to keep in mind condition (8) to avoid a non-desirable blurring of distribution.

It should be noted that for practical application of the effect under investigation, high values of ε_a are needed. It takes values $\varepsilon_a \sim 0.001$–0.01 at wavelengths approximately equal to be considered here to be used in magneto-optics materials frequently [29]. Faraday rotation angle and Verdet constant are used frequently used for characterizing gyrotropic materials. Faraday rotation angle may be defined as follows [43]: $\theta_F = z\omega[(\varepsilon + \varepsilon_a)^{1/2} - (\varepsilon - \varepsilon_a)^{1/2}]/(2c) = BVz$, where B is the external magnetic induction and V is the Verdet constant. For $\varepsilon_a << \varepsilon$, gyrotopy is proportional to BV. The high values of Verdet constant in the THz frequency range (0.1–10 THz) have some semiconductors: (Cd,Mn)Te (10^3 rad T^{-1} m^{-1}) [46], InSb (10^4 rad T^{-1} m^{-1}) [47], HgTe (10^6 rad T^{-1} m^{-1}) [48]. In such materials, the values of ε_a may be reached, which are necessary for practical application, but proposed structure should be redesigned for THz frequencies (radius of the core should be increased). We should note that at THz frequencies propagation length of SPPs is much greater than in infrared domain as considered here. Thus, it is possible to achieve a greater rotation angles but at greater scales.

4. Spiral graphene-based waveguides

Let us consider a dielectric cylinder (core of the waveguide) with dielectric permittivity $\varepsilon_{in} = \varepsilon^r_{in}\varepsilon_0$ (ε_0 is the electric constant) and radius R, which is coiled by graphene strip (see **Figure 4a** and **b**). Such cylinder is embedded in the dielectric medium with dielectric permittivity $\varepsilon_{out} = \varepsilon^r_{out}\varepsilon_0$. Both mediums will be considered as non-magnetic ($\mu_{in} = \mu_{out} = \mu_0$). We will use cylindrical coordinates (r, ϕ, z). Let us suppose that the z-axis coincides with the cylinder axis.

The net of cylindrical surface may be represented as meta-surface formed by graphene strips with width W and spacer width G (see **Figure 4c**). Such meta-surface may be described by 2D conductivity tensor $\hat{\sigma}$ of which components depend on the tilt angle θ [49, 50]:

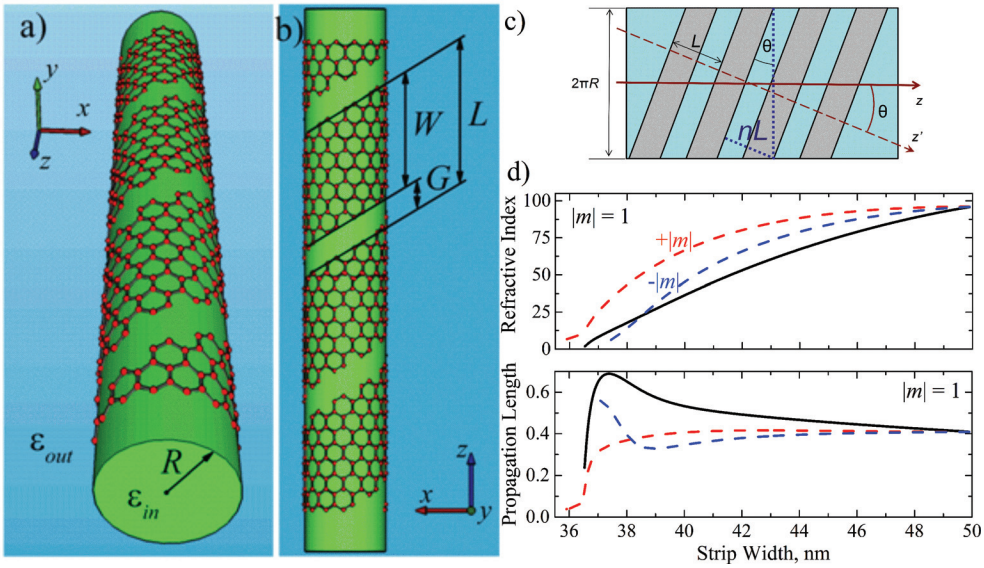

Figure 4. Geometry of the problem. Perspective (a) and top projection (b) views of the part of the meta-tube. Schemes illustrating the coupling between the tilt angle θ and tilt number n (c) and influence of the graphene strip width W on dispersion characteristic of the plasmonic modes with $m = \pm 1$ (d), $n = 0$ for the solid line corresponds to the non-chiral structure formed by graphene rings, $n = 9$ for dashed lines approximately corresponds to the tilt angle 45°.

$$\hat{\sigma}_g = \begin{pmatrix} \sigma_{\phi\phi} & \sigma_{\phi z} \\ \sigma_{z\phi} & \sigma_{zz} \end{pmatrix}$$

$$\sigma_{\phi\phi} = \frac{L\sigma_g\sigma_C \sin^2\theta}{W\sigma_C + G\sigma_g} + \frac{W}{L}\sigma_g \cos^2\theta,$$

$$\sigma_{zz} = \frac{L\sigma_g\sigma_C \cos^2\theta}{W\sigma_C + G\sigma_g} + \frac{W}{L}\sigma_g \sin^2\theta, \tag{9}$$

$$\sigma_{\phi z} = \sigma_{z\phi} = \left(\frac{W}{L}\sigma_g - \frac{L\sigma_g\sigma_C}{W\sigma_C + G\sigma_g}\right)\sin\theta\cos\theta$$

$$\sigma_C = -i\omega\varepsilon_0\varepsilon\left(\frac{L}{\pi}\right)\ln\left[\csc\left(\frac{\pi G}{2L}\right)\right]$$

In Eq. (9), σ_g is the graphene conductivity, which may be divided into intra- and inter-band contributions $\sigma_g = \sigma_{\text{intra}} + \sigma_{\text{inter}}$, while σ_C is the effective meta-surface conductivity caused by capacitive coupling between graphene strips. Such representation is valid when the wavelength of electromagnetic wave is much longer than the periodicity of the structure.

For fixed periodicity of the surface $L = W + G$, the tilt angle may get discrete values: $\theta_n = \arcsin[nL/2\pi R]$, where n is an integer number, which may be interpreted as the count of graphene spirals (or the count of spacers in the meta-surface between two enclosed strip edges). We will call this number the 'tilt number'.

For investigation of electrodynamics of such structure, one should solve Maxwell's equations inside each medium taking into account the boundary conditions: $E_{z,}^{\text{in}} = E_z^{\text{out}}$, $E_\varphi^{\text{in}} = E_\varphi^{\text{out}}$, $H_z^{\text{out}} - H_z^{\text{in}} = -\sigma_{\phi\phi}E_\phi^{\text{in}} - \sigma_{\phi z}E_z^{\text{in}}$ and $H_\phi^{\text{out}} - H_\phi^{\text{in}} = \sigma_{zz}E_z^{\text{in}} + \sigma_{z\phi}E_\phi^{\text{in}}$. Considering the waves propagating along the cylinder axis, one may put electric and magnetic fields $\mathbf{E}, \mathbf{H} \sim \exp[-i\omega t + ihz + im\phi]$, where ω is the circular frequency, h is the propagation constant and m is the azimuthal mode index.

The calculations show that propagation constants for the modes propagating along the z-axis with opposite azimuthal rotation direction (we will denote these propagation constants as $h_{+|m|}$ and $h_{-|m|}$) are different, similarly to the plasmonic modes in gyrotropic graphene-covered nanowires (see Section 3). Thus, if one has azimuthal field distribution at an input of the waveguide $z = 0$ proportional to $\cos[m\phi]$, at the output $z = z_0$ one will have rotated field distribution. Rotation angle may be calculated as $\psi = z_0(\text{Re}[h_{-|m|}] - \text{Re}[h_{+|m|}])/2|m|$, while $z_0|\text{Im}[h_{-|m|}] - \text{Im}[h_{+|m|}]| \ll 1$. To characterize the rotation effect, we will also use the specific rotation angle $\psi_0 = \psi/z_0$.

Figure 4(d) shows the dispersion characteristics (mode refractive index $\text{Re}[h_m]/k_0$ and the propagation length $1/2\text{Im}[h_m]$) for the structure formed by graphene strip with the periodicity $L = 50$ nm, core radius $R = 100$ nm for the frequency of electromagnetic wave $f = 50$ THz via graphene strip width for the modes with $m = \pm 1$ and two values of the tilt angles ($n = 0$ corresponds to the non-chiral structure formed by graphene rings, $n = 9$ approximately corresponds to the tilt angle 45°). We assume that $\varepsilon^r{}_{\text{in}} = 3$, and $\varepsilon^r{}_{\text{out}} = 1$. For the fixed periodicity L, a decrease in strip width leads to an increase in the spacer width. One can see that there is a critical strip width when the structure cannot support plasmonic mode. This critical width is different for a different mode index m. For non-zero tilt number modes with the opposite azimuthal rotation directions (i.e. $\pm|m|$) have different critical width. The mode rotating in the same direction as chirality of the structure exists at lower graphene width but has low propagation length, while the opposite mode has a bulk behaviour when graphene width reaches the critical value.

Figure 5 shows the specific rotation angle for the spiral waveguide with the periodicity $L = 50$ nm, graphene strip width $W = 45$ nm and the spacer width $G = 5$ nm via the tilt number of the structure. Other parameters are the same as for **Figure 2**. One can see that at $n < n_{\text{cr}} \approx 10$, specific rotation angle of lower modes is greater than that of higher modes. At $n > n_{\text{cr}}$, the opposite behaviour take a place. Maximal specific rotation reaches up to few hundreds of degrees, and it is observed near the tilt angle of about $\pi/4$, when non-diagonal components of conductivity are maximal, similarly to the TE-TM coupling for the fundamental plasmonic mode. The maximums of higher modes are shifted to greater tilt angles. We should note that the rotation angle strictly depends on the graphene chemical potential, which may be controlled by gate voltage or chemical doping. The maximal values of the specific rotation angle are much higher than that of gyrotropic graphene-covered nanowires for the similar set of parameters (see Section 3). Negative tilt numbers (and tilt angles) correspond to the opposite chirality of the structure. Such situation will be observed for the backward waves propagating in the structure, and the specific rotation angle will have negative values. Thus, the structure is strictly non-reciprocal. This property may be used for one-way wave propagation if we have graphene strip width lower than the critical one for the negative azimuthal mode index: mode

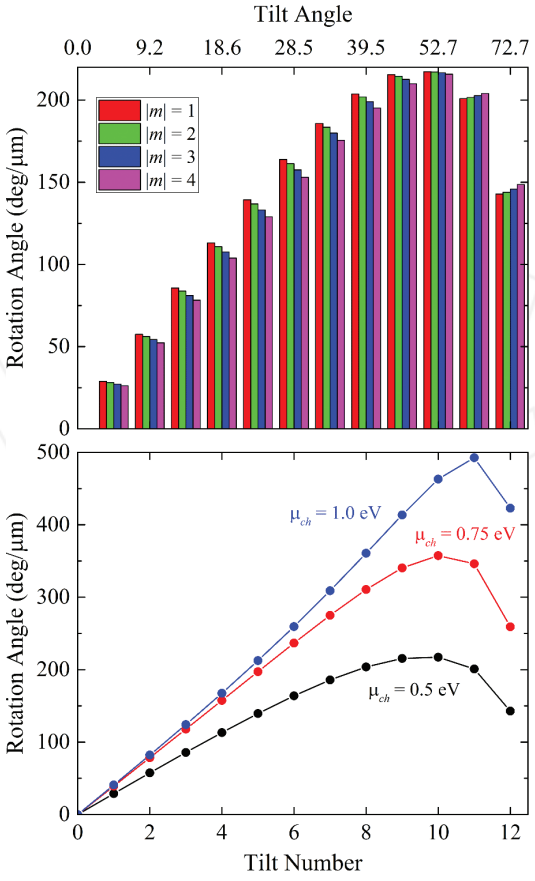

Figure 5. Specific rotation angle for the spiral waveguide with the periodicity $L = 50$ nm, graphene strip width $W = 45$ nm and the spacer width $G = 5$ nm via the tilt number (or the tilt angle) of the structure. The upper panel shows the specific rotation angle for first four modes for graphene chemical potential $\mu_{ch} = 0.5$ eV. The lower panel shows the specific rotation angle for the mode with $|m| = 1$ for different values of graphene chemical potential.

with the positive azimuthal index will still propagate along the structure, while in the opposite direction only the mode with the negative azimuthal index will propagate.

One may see that even at maximal possible tilt angle the specific rotation angle is still high enough. This fact makes the concept of surface plasmon-polaritons control by the shear strains very promising for practical applications. Let us imagine that we have a non-chiral structure formed by nanowire longitudinally covered by graphene strips (see **Figure 6**). This situation corresponds to the tilt angle $\theta = 90^{o}$. Non-diagonal components of the surface conductivity tensor will be equal to zero, and no rotation of high-order plasmonic modes will be observed. If shear strains are applied to such a structure, the spiral waveguide will be formed with the tilt angle defined by the strain value and field distribution at the output of the waveguide will be rotated.

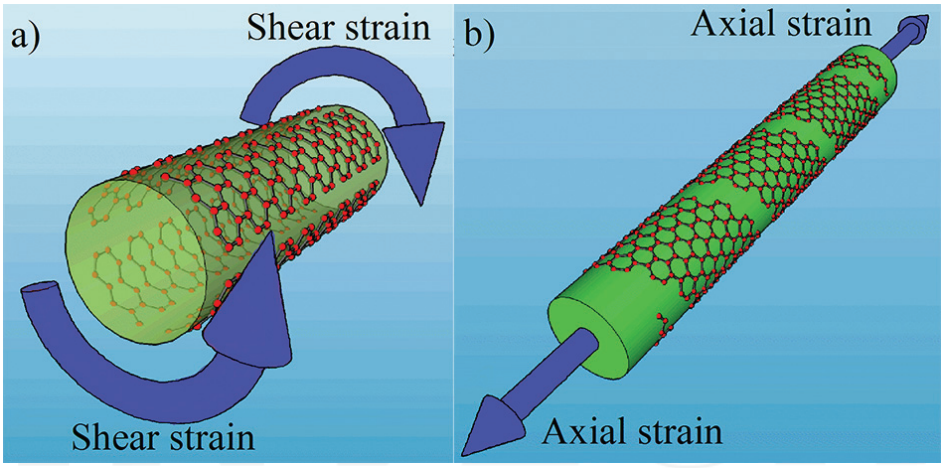

Figure 6. The schemes illustrating formation of the spiral waveguide by shear strains (a) and control of spiral waveguide parameters by axial strains (b).

Another way to control plasmons in the structure under investigation by external strains is to apply an axial strain to the structure. An axial strain will lead to the change in the spacer width G and the periodicity of the structure L. From Eq. (9), we may see that the relation W/L affects significantly the meta-surface conductivity. In the situation under discussion W/L may be controlled by the axial strain. It is seen from **Figure 4(d)** that even a change in the strip width on some nanometres leads to a significant difference in the propagation constants of counterrotating azimuthal modes. Thus, proposed structure should be very sensitive to an axial stresses.

5. Concluding remarks

In this chapter, we have investigated in detail two ways of breaking of the degeneracy of the plasmonic modes with the opposite azimuthal rotations for graphene-coated nanowires: by external magnetic field and by surface spiral structure. This breaking of the degeneracy may lead to a giant spatial rotation of high-order plasmonic modes, and to the redistribution of the intensity of electromagnetic wave.

The open problem is the self-consistent problem of SPPs propagation in plasmonic magnetic nanowires. Magnetization of the nanowire, in general, will lead to the change in SPPs properties, while SPPs themselves will induce an effective magnetic field, which will change the magnetization of the nanowire. This effect should be taken into account especially for nonlinear SPPs. To the best of our knowledge, this problem is still unsolved.

The effects discussed in Section 4 are caused by the off-diagonal components of the surface conductivity tensor. In addition to the considered structure, some similar effect may be observed for the nanowires covered by strained graphene layer. Recent investigation of

graphene conductivity under a non-mechanical distortion shows that it may have anisotropic conductivity tensor with the off-diagonal components as well [51]. This fact opens the door for further investigations of SPPs control by artificial strains.

The predicted effects may play a crucial role in the polarization rotation in metamaterials consisting of multiple proposed structures. On the other hand, redistribution of the electromagnetic wave intensity may be interpreted in terms of local change in the photonic density of states, which may be used to control the radiation of quantum dots placed near such plasmonic nanowire. These results open the door to novel plasmonic applications ranging from nanowire-based Faraday isolators and one-way devices to the magnetic and strain control in quantum-optical applications.

Acknowledgements

The work was supported in part by Stratégie internationale NNN-Telecom de la Région Pays de La Loire, Alexander von Humboldt Stiftung, President of Russian Federation (project # MK-1653.2017.2), Russian Foundation for Basic Research (grants ## 16-37-00023, 16-07-00751 and 16-29-14045), and Act 211 Government of the Russian Federation (contract No 02.A03.21.0011).

Author details

Dmitry A. Kuzmin[1]*, Igor V. Bychkov[1], Vladimir G. Shavrov[2] and Vasily V. Temnov[3]

*Address all correspondence to: kuzminda@csu.ru

1 Chelyabinsk State University, Chelyabinsk, Russian Federation

2 Kotel'nikov Institute of Radio-Engineering and Electronics of RAS, Moscow, Russian Federation

3 Institut des Molécules et Matériaux du Mans, Université du Maine, France

References

[1] Bao Q., Loh K.P. Graphene photonics, plasmonics, and broadband optoelectronic devices. ACS Nano. 2012;**6**(5):3677–3694. DOI: 10.1021/nn300989g

[2] Grigorenko A.N., Polini M., Novoselov K.S. Graphene plasmonics. Nature Photonics. 2012;**6**:749–758. DOI: 10.1038/nphoton.2012.262

[3] Garcia de Abajo F.J. Graphene plasmonics: challenges and opportunities. ACS Photonics. 2014;**1**(3):135–152. DOI: 10.1021/ph400147y

[4] Mikhailov S.A., Ziegler K. New electromagnetic mode in graphene. Physical Review Letters. 2007;**99**:016803. DOI: 10.1103/PhysRevLett.99.016803

[5] Hanson G.W. Quasi-transverse electromagnetic modes supported by a graphene parallel-plate waveguide. Journal of Applied Physics. 2008;**104**(8):084314. DOI: 10.1063/1.3005881

[6] Bludov Y.V., Ferreira A., Peres N.M.R., Vasilevskiy M. A primer on surface plasmon-polaritons in graphene. International Journal of Modern Physics B. 2013;**27**(10):1341001. DOI: 10.1142/S0217979213410014

[7] Kotov O.V., Kol'chenko M.A., Lozovik Y.E. Ultrahigh refractive index sensitivity of TE-polarized electromagnetic waves in graphene at the interface between two dielectric media. Optics Express. 2013;**21**(11):13533–13546. DOI: 10.1364/OE.21.013533

[8] Buslaev P.I., Iorsh I.V., Shadrivov I.V., Belov P.A., Kivshar Y.S. Plasmons in waveguide structures formed by two graphene layers. JETP Letters. 2013;**97**(9):535–539. DOI: 10.1134/S0021364013090063

[9] Smirnova D.A., Iorsh I.V., Shadrivov I.V., Kivshar Y.S. Multilayer graphene waveguides. JETP Letters. 2014;**99**(8):456–460. DOI: 10.1134/S002136401408013X

[10] Koppens F.H.L., Chang D.E., García de Abajo F.J. Graphene plasmonics: a platform for strong light–matter interactions. Nano Letters. 2011;**11**(8):3370–3377. DOI: 10.1021/nl201771h

[11] Yan H., Low T., Zhu W., Wu Y., Freitag M., Li X., Guinea F., Avouris P., Xia F. Damping pathways of mid-infrared plasmons in graphene nanostructures. Nature Photonics. 2013;**7**:394–399. DOI: 10.1038/nphoton.2013.57

[12] Soto Lamata I., Alonso-Gonzalez P., Hillenbrand R., Nikitin A.Y. Plasmons in cylindrical 2D materials as a platform for nanophotonic circuits. ACS Photonics. 2015;**2**(2):280–286. DOI: 10.1021/ph500377u

[13] Gao Y., Ren G., Zhu B., Liu H., Lian Y., Jian Sh. Analytical model for plasmon modes in graphene-coated nanowire. Optics Express. 2014;**22**(20): 24322–24331. DOI: 10.1364/OE.22.024322

[14] Gao Y., Ren G., Zhu B., Wang J., Jian Sh. Single-mode graphene-coated nanowire plasmonic waveguide. Optics Letters. 2014;**39**(20):5909–5912. DOI: 10.1364/OL.39.005909

[15] Correas-Serrano D., Gomez-Diaz J.S., Alu A., Alvarez-Melcon A. Electrically and magnetically biased graphene-based cylindrical waveguides: analysis and applications as reconfigurable antennas. IEEE Transactions on Terahertz Science and Technology. 2015;**5**(6): 951–960. DOI: 10.1109/TTHZ.2015.2472985

[16] Kuzmin D.A., Bychkov I.V., Shavrov V.G., Kotov L.N. Transverse-electric plasmonic modes of cylindrical graphene-based waveguide at near-infrared and visible frequencies. Scientific Reports. 2016;**6**: 26915. DOI: 10.1038/srep26915

[17] Krasavin A.V., Zheludev N.I. Active plasmonics: controlling signals in Au/Ga waveguide using nanoscale structural transformations. Applied Physics Letters. 2014;**84**(8):1416. DOI: 10.1063/1.1650904

[18] Fedutik Y., Temnov V.V., Schöps O., Woggon U., Artemyev M.V. Exciton-plasmon-photon conversion in plasmonic nanostructures. Physical Review Letters. 2007;**99**:136802. DOI: 10.1103/PhysRevLett.99.136802

[19] Temnov V.V., Armelles G., Woggon U., Guzatov D., Cebollada A., Garcia-Martin A., et al. Active magneto-plasmonics in hybrid metal–ferromagnet structures. Nature Photonics. 2010;**4**:107–111. DOI: 10.1038/nphoton.2009.265

[20] LeBlanc S.J., McClanahan M.R., Jones M., Moyer P.J. Enhancement of multiphoton emission from single CdSe quantum dots coupled to gold films. Nano Letters. 2013;**13**(4):1662–1669. DOI: 10.1021/nl400117h

[21] Abbasi F., Davoyan A.R., Engheta N. One-way surface states due to nonreciprocal light-line crossing. New Journal of Physics. 2015;**17**:063014. DOI: 10.1088/1367-2630/17/6/063014

[22] Kuzmin D.A., Bychkov I.V., Shavrov V.G. Magnetic field control of plasmon polaritons in graphene-covered gyrotropic planar waveguide. Optics Letters. 2015;**40**(11):2557–2560. DOI: 10.1364/OL.40.002557

[23] Kurkin M.I., Bakulina N.B., Pisarev R.V. Transient inverse Faraday effect and ultrafast optical switching of magnetization. Physical Review B. 2008;**78**:134430. DOI: 10.1103/PhysRevB.78.134430

[24] Mentink J.H., Hellsvik J., Afanasiev D.V., Ivanov B.A., Kirilyuk A., Kimel A.V., et al. Ultrafast spin dynamics in multisublattice magnets. Physical Review Letters. 2012;**108**:057202. DOI: 10.1103/PhysRevLett.108.057202

[25] Kirilyuk A., Kimel A.V., Rasing T. Laser-induced magnetization dynamics and reversal in ferrimagnetic alloys. Reports on Progress in Physics. 2013;**76**(2):026501. DOI: 10.1088/0034-4885/76/2/026501

[26] Kurkin M.I., Orlova N.B. Femtosecond magnetooptics and ultrafast magnetization reversal of ferromagnetic. Journal of Magnetism and Magnetic Materials. 2014;**361**:224–231. DOI: 10.1016/j.jmmm.2014.02.079

[27] Belotelov V.I., Doskolovich L.L., Zvezdin A.K. Extraordinary magneto-optical effects and transmission through metal-dielectric plasmonic systems. Physical Review Letters. 2007;**98**:077401. DOI: 10.1103/PhysRevLett.98.077401

[28] Belotelov V.I., Akimov I.A., Pohl M., Kotov V.A., Kasture S., Vengurlekar A.S., et al. Enhanced magneto-optical effects in magnetoplasmonic crystals. Nature Nanotechnology. 2011;**6**:370–376. DOI: 10.1038/nnano.2011.54

[29] Kreilkamp L.E., Belotelov V.I., Chin J.Y., Neutzner S., Dregely D., Wehlus T., et al. Waveguide-plasmon polaritons enhance transverse magneto-optical Kerr effect. Physical Review X. 2013;**3**:041019. DOI: 10.1103/PhysRevX.3.041019

[30] Khokhlov N.E., Prokopov A.R., Shaposhnikov A.N., Berzhansky V.N., Kozhaev M.A., Andreev S.N., et al. Photonic crystals with plasmonic patterns: novel type of the heterostructures for enhanced magneto-optical activity. Journal of Physics D: Applied Physics. 2015;**48**(9):095001. DOI: 10.1088/0022-3727/48/9/095001

[31] Razdolski I., Parchenko S., Stupakiewicz A., Semin S., Stognij A., Maziewski A., et al. Second-harmonic generation from a magnetic buried interface enhanced by an interplay of surface plasma resonances. ACS Photonics. 2015;**2**(1):20–26. DOI: 10.1021/ph500382u

[32] Baranova N.B., Zel'dovich B.Y. Rotation of a ray by a magnetic field. JETP Letters. 1994;**59**(10):681–684.

[33] Darsht M.Y., Zhirgalova I.V., Zel'dovich B.Y., Kundikova N.D. Observation of a "magnetic" rotation of the speckle of light passed through an optical fiber. JETP Letters. 1994;**59**(11):763–765.

[34] Ardasheva L.I., Sadykova M.O., Sadykov N.R., Chernyakov V.E. Rotation of the speckle pattern in a low-mode optical fiber in a longitudinal magnetic field. Journal of Optical Technology. 2002;**69**(7):451. DOI: 10.1364/JOT.69.000451

[35] Ardasheva L.I., Kundikova N.D., Sadykova M.O., Sadykov N.R., Chernyakov V.E. Speckle-pattern rotation in a few-mode optical fiber in a longitudinal magnetic field. Optics and Spectroscopy. 2003;**95**(4):645–651. DOI: 10.1134/1.1621451

[36] Kuzmin D.A., Bychkov I.V., Shavrov V.G. Influence of graphene coating on speckle-pattern rotation of light in gyrotropic optical fiber. Optics Letters. 2015;**40**(6):890–893. DOI: 10.1364/OL.40.000890

[37] Kuzmin A., Bychkov I.V., Shavrov V.G., Temnov V.V. Giant Faraday rotation of high-order plasmonic modes in graphene-covered nanowires. Nano Letters. 2016;**16**(7):4391–4395. DOI: 10.1021/acs.nanolett.6b01517

[38] Hanson G.W. Dyadic Green's functions and guided surface waves for a surface conductivity model of graphene. Journal of Applied Physics. 2008;**103**(6):064302. DOI: 10.1063/1.2891452

[39] Falkovsky L.A., Varlamov A.A. Space-time dispersion of graphene conductivity. The European Physical Journal B. 2007;**56**(4):281–284. DOI: 10.1140/epjb/e2007-00142-3

[40] Falkovsky L.A. Optical properties of graphene and IV–VI semiconductors. Physics-Uspekhi. 2008;**51**(9):887–897. DOI: 10.1070/PU2008v051n09ABEH006625

[41] Kuzmin D.A., Bychkov I.V., Shavrov V.G., Temnov V.V., Lee H.I., Mok J. Plasmonically induced magnetic field in graphene-coated nanowires. Optics Letters. 2016;**41**(2):396–399. DOI: 10.1364/OL.41.000396

[42] Suhl H., Walker L.R. Topics in guided-wave propagation through gyromagnetic media: Part I—The completely filled cylindrical guide. Bell System Technical Journal. 1954;**33**(5):579–659. DOI: 10.1002/j.1538-7305.1954.tb02358.x

[43] Gurevich A.G., Melkov G.A. Magnetization oscillations and waves. Boca Raton: CRC Press; 1996. 445 p.

[44] Cojocaru E. Modes in dielectric or ferrite gyrotropic slab and circular waveguides, longitudinally magnetized, with open and completely or partially filled wall. Journal of the Optical Society of America B. 2010;**27**(10):1965–1977. DOI: 10.1364/JOSAB.27.001965

[45] Thongrattanasiri S., Manjavacas A., García de Abajo F.J. Quantum Finite-Size Effects in Graphene Plasmons. ACS Nano. 2012;**6**(2):1766–1775. DOI: 10.1021/nn204780e

[46] Gaj J.A., Galazka R.R., Nawrocki M. Giant exciton Faraday rotation in Cd1-xMnxTe mixed crystals. Solid State Communications. 1978;**25**(3):193–195. DOI: 10.1016/0038-1098(78)91477-1

[47] Palik E.D., Furdyna J.K. Infrared and microwave magnetoplasma effects in semiconductors. Reports on Progress in Physics. 1970;**33**(3):1193. DOI: 10.1088/0034-4885/33/3/307

[48] Shuvaev A.M., Astakhov G.V., Pimenov A., Brüne C., Buhmann H., Molenkamp L.W. Giant magneto-optical Faraday effect in HgTe thin films in the terahertz spectral range. Physical Review Letters. 2011;**106**:107404. DOI: 10.1103/PhysRevLett.106.107404

[49] Gomez-Diaz J.S., Tymchenko M., Alù A. Hyperbolic plasmons and topological transitions over uniaxial metasurfaces. Physical Review Letters. 2015;**114**:233901. DOI: 10.1103/PhysRevLett.114.233901

[50] Gomez-Diaz J.S., Tymchenko M., Alù A. Hyperbolic metasurfaces: surface plasmons, light-matter interactions, and physical implementation using graphene strips. Optical Materials Express. 2015;**5**(10):2313–2329. DOI: 10.1364/OME.5.002313

[51] Oliva-Leyva M., Naumis G.G. Effective Dirac Hamiltonian for anisotropic honeycomb lattices: optical properties. Physical Review B. 2016;**93**:035439. DOI: 10.1103/PhysRevB.93.035439